Fifth South African Conference on Computational and Applied Mechanics
SACAM06
Cape Town, 16-18 January 2006


# ULTRASONIC DETECTION OF CRACKS IN UNIAXIAL GLASS FIBRE RODS

**Derren Wood and Philip Loveday**

Sensor Science and Technology, CSIR Materials Science and Manufacturing,
Box 395, Pretoria 0001, South Africa, dwood@csir.co.za, ploveday@csir.co.za

## Abstract

A non-destructive examination procedure based on a guided wave inspection approach is used for the acoustic examination of glass fibre reinforced composite rods. This paper contains an investigation into the characteristics of guided wave propagation in the rods. We attempt to model the excitation and transmission of waves along undamaged as well as damaged rods in order to predict the received signals, and we compare the model results with experimental data. Specially developed waveguide finite elements are used to determine the wave propagation characteristics of the rod. This yields an understanding of its wave dispersion characteristics and allows for the selection of appropriate excitation modes. Conventional transient finite element modelling is performed in order to determine what effects cracks have on the passage of the induced waves, and therefore also on the eventual output signals. Additionally, the determination of crack reflection coefficients is discussed.

**Key words:** Waveguide analysis, dispersion, finite element analysis.

## 1. Introduction

This paper outlines a study into the use of ultrasonic guided waves for the inspection of the glass fibre reinforced polymer rods used as high voltage insulator cores. GFRP rods are increasingly used as an alternative to ceramics in the construction of insulators for high voltage power lines, and also as an alternative to steel reinforcing rods in concrete. The composite rods that are used as electrical insulator cores support large tensile loads. Screening these rods for defects such as cracks or pores has become important both from a safety and cost perspective. Ultrasonic NDE techniques offer a means of detecting internal and/or surface damage in composites which is safe, quick and relatively cost effective. Various ultrasonic techniques have been applied in the past to detect defects in composite media, the most well known being perhaps the passive acoustic emission technique and the active ultrasonic A, B and C scans. Steiner et al. [1] for instance, compared acoustic emission, ultrasonic C-scans and polar backscattering scans on the basis of their relevance and accuracy for the determination of the progression of matrix cracks in composite laminates and in Prevorovsky et al. [2] a study is discussed in which acoustic emission and ultrasonic C-scanning are used to determine the damage state of composite tubes. In the current study, an active approach was necessitated since a requirement is to detect defects already present in the material, so acoustic emission is inappropriate. The application of the active scanning techniques to the detection of damage in the GFRP cores is complicated by the fact that the cores are surrounded by an awkwardly shaped protective rubber sheath. Only the ends of the

cores are left free for the application and/or sensing of a signal. An alternative method of ultrasonic inspection that was found to be applicable to the current study is guided wave inspection. Conventional ultrasonic NDT makes use of bulk waves that travel in unbounded media while guided wave inspection requires the presence of a boundary or interface. Various types of waves exist in bounded structures and can be used for guided wave inspection, including Rayleigh waves (on a surface), Lamb waves (in plates) and Stoneley waves (at the interface between two materials). A review of research and development in this area is discussed in Rose [3], which lists numerous practical applications of guided wave inspection. An advantage of guided wave inspection is that it can be performed over long distances, either from a single probe (pulse-echo mode) or between two probes (transmission mode). It is possible to test coated, insulated or buried structures by removing only a small portion of the coating to gain access to the structure. Parts of a structure which are inaccessible may then be interrogated with guided waves. The interaction of guided waves with damage in metal structures has been studied extensively, primarily by a research group based at Imperial College, London [4, 5] and inspection systems utilizing guided waves have been implemented successfully [6, 7]. A system for the detection of complete breaks in railway lines has been developed in South Africa [8]. Guided waves have also been applied to damage detection in composite plates [9]. Many researchers apply finite element analysis for the investigation of wave propagation in waveguides. Conventional finite element codes are applied to perform time-domain simulations. These transient analyses are computationally demanding as a fairly long section of waveguide has to be modelled to allow far-field behaviour to be realized and to avoid the effects of reflections from the ends of the model. Gavrić [10] applied a more elegant finite element procedure to compute the propagative waves in rails. In his method, a complex exponential function was used to represent the displacement variation along the waveguide and finite element discretisation was applied over the cross-section. This results in a two-dimensional mesh, which is capable of modelling the wave propagation along the waveguide. This approach is very efficient from a computational point-of-view. Another formulation of the element is suggested in Hayashi et al. [11]. The remainder of this paper is structured as follows: In Section 2 the nature of guided wave propagation in undamaged rods is addresses, the experimental setup is described and a comparison is drawn between measured data and numerical results. In Section 3 the calculation of reflection coefficients is discussed and results of the analyses of rods containing damage are presented. Concluding remarks appear in Section 4.

## 2. Modelling and measurement of wave propagation in composite rods

### 2.1. Modelling

The waveguide finite elements developed by Gavrić [10] have been implemented at the CSIR and were used to determine the types of waves that would exist in a GFRP rod. Understanding what waves exist and how they can change as a function of frequency is the first requirement in developing a guided wave inspection system. Figure 1 shows the wavenumber vs. frequency and group velocity vs. frequency curves which characterize the wave propagation behaviour within the insulator core rods. Each curve represents a travelling wave mode. Below 70 kHz only four modes exist in the rod. Two are bending modes (one for each non-axial dimension) whose curves coincide, the third is a torsional mode and the fourth, which has the highest wave speed in this region, is an axial mode. Points on the curves can also be calculated as eigenvalue solutions to conventional axisymmetric or three dimensional finite element models with appropriate boundary conditions. Figure 2, for instance, shows a

bending mode at 1 kHz. From the length of the model, the wavenumber can be calculated and used for comparison with the waveguide results. Table 1 shows such a comparison. As can be seen, the waveguide solutions agree more closely with the theoretically expected results than the conventional FEM results. The waveguide finite element solution also yields the mode shapes associated with a mode. By mode shapes we mean the maximum displacement and phase of points on the wave-guide cross-section and these shapes too, change as a function of frequency. Figure 3 shows the in plane and axial displacements associated with two points on the curves in Figure 1. The first belongs to an axisymmetric mode, whereas the second exhibits a more complicated, non-axisymmetric displacement field.

## 2.2. Measurement

Since it is impossible to excite a wave packet containing only one discrete frequency, any physically excited signal in the rod will inevitably be composed of a band of frequencies. If there is a significant variation in the velocities associated with the frequency components in the band, the wave will tend to elongate as it travels down the waveguide. This elongation is known as dispersion. In Figure 1, one notices that the group velocities of the waves are not constant with frequency for any of the modes, save the torsional mode. However, there are regions wherein certain of the modes have a nearly constant group velocity. For practical testing, it is desirable to work in these regions if one wants to avoid the complications caused by dispersion. A further practical complication is that at any particular frequency the rod will support more than one travelling mode. Hence it is desirable to excite only the selected non-dispersive mode while suppressing the others. This may in general place constraints on the design of the excitation transducer. For the present study it was decided to work in the region below 80 kHz, where the first axial mode is relatively non-dispersive. A simple piezoelectric disc was used as a transducer, which was attached to the end of the rod and excites axisymmetrically, the motion being primarily axial. Since the other two modes in this region are not axisymmetric, they could not be present in the excited pulse, and the axial mode could be successfully isolated.

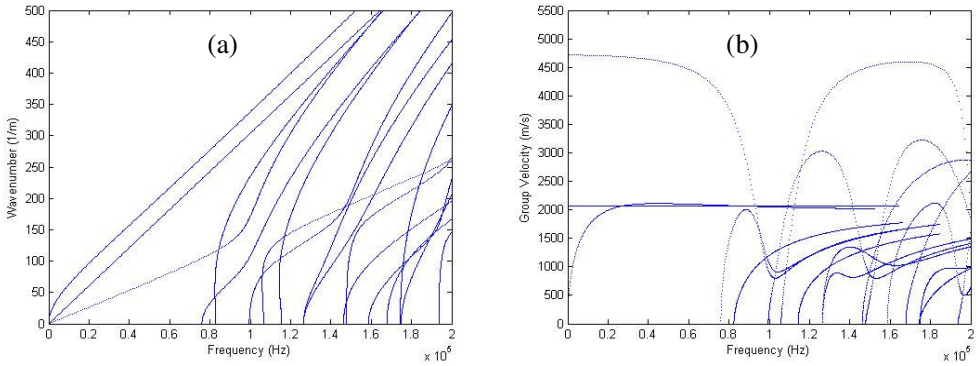


**Figure 1.** Dispersion curves, (a) wavenumber vs. frequency, (b) group velocity vs. frequency.

| Mode | Waveguide FE (Hz) | 3-D FE (Hz) | Axisymmetric FE (Hz) | 1-D Theory (Hz) |
|---|---|---|---|---|
| Bending | 114 | 114 | - | 114 |
| Torsion | 2054 | 2009 | - | 2054 |
| Axial | 4547 | 4857 | 4551 | 4547 |

**Table 1.** Comparison of modal frequencies at specific wavenumbers.

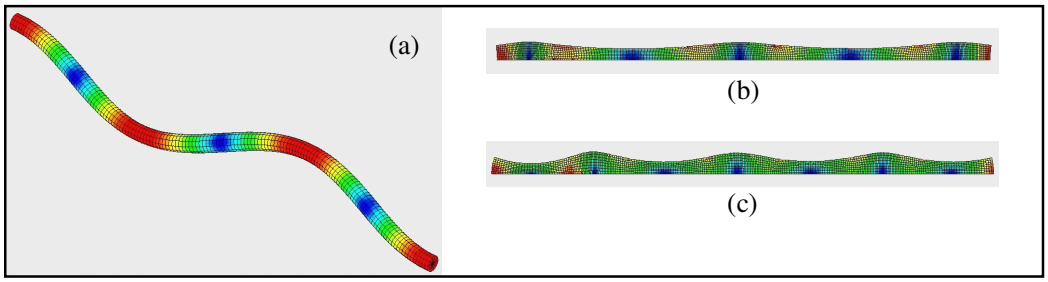


**Figure 2.** (a) Bending mode (1 kHz), (b) axisymmetric mode (39 kHz), (c) axisymmetric mode (61kHz).

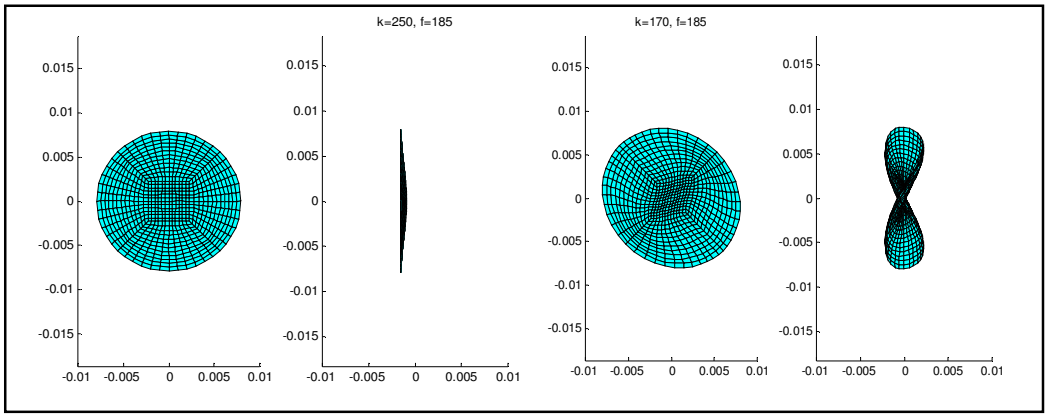


**Figure 3.** Mode shapes deduced using waveguide finite elements.

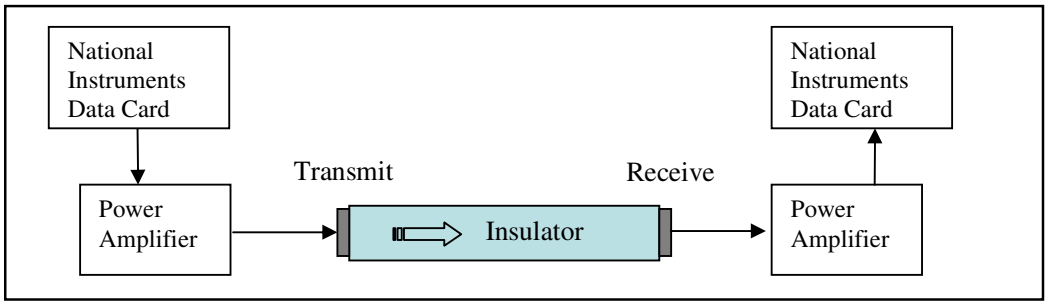


**Figure 4.** Experimental setup.

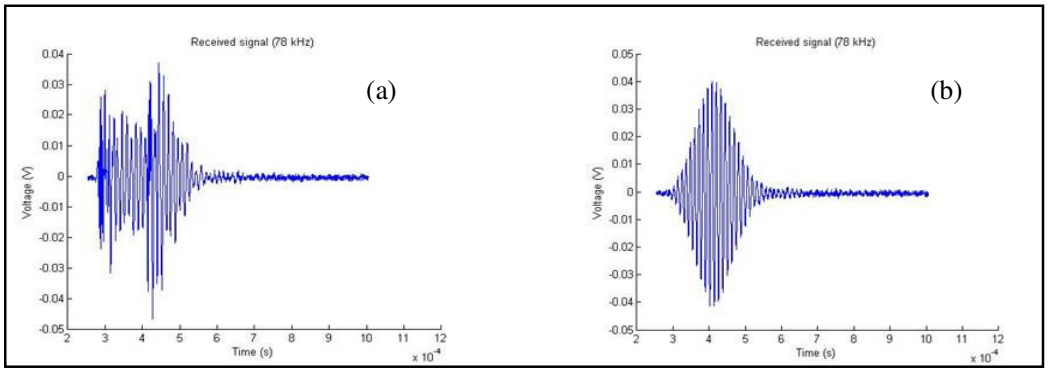


**Figure 5.** Measured responses to different excitation waveforms, (a) response to sinusoidal excitation, (b) response to windowed excitation signal (Hanning window).

Experimental setup

The experimental set up used in the experiments uses a National Instruments data acquisition card together with LabView software both to generate arbitrary input signals and to capture and interpret the received signals. Figure 4 is a schematic of the experimental set up. Signals between 30 kHz and 80 kHz were transmitted through the rod. Two types of signals were used. The first was a normal sinusoidal signal that started and stopped abruptly and the other was a tone-burst signal produced by windowing the sine-wave with a Hanning function. The windowed signal produced clearer measured responses (see Figure 5) because the discontinuous voltage at the start and end of the sine input tends to produce high frequency responses in the rod that complicate the output signals in much the same way that noise does. This leads to the conclusion that using windowed driving function is a better option for detection purposes. Initially, the core of a long (1.36m) insulator was tested so that the wave propagation characteristics of the rod could be recorded and modelled. In the current study, modelling and analysing the attenuation of signals due to the rubber covering has been avoided, so the rubber insulation was removed. The end fittings attached to the insulator core were also removed and piezoelectric actuator discs were bonded to the ends of the rod. Experiments were carried out at a number of frequencies on an undamaged rod to assess the effects of dispersion experimentally. Damage was then introduced into the rod in the form of an axisymmetric notch, and the tests were repeated.

### 2.3. Comparison of results from an undamaged rod

The wave propagation behaviour depicted in the curves in Figure 1 is very sensitive to the material properties. Without a precise knowledge of both the piezoelectric properties of the disc and the five constitutive properties of the transversely isotropic rod, it is difficult to accurately model the test data quantitatively. However, by iterating on the rod's material properties and comparing the model results with the test results on the basis of wave arrival time and dispersion, it is possible to model the wave propagation characteristics qualitatively, at least for the axial mode considered. Figure 6 shows measurement data for the rod excited by windowed pulses of various frequencies. The figures depict signals detected at one end of the rod; the input signal being applied to the other. Successive wave packets are detected corresponding to successive arrivals (reflections) of the excitation wave packet. All the signals suffer a decrease in amplitude related in part to the rod's internal damping and in part to the dispersion of the wave. The signals at higher frequencies, though, clearly show elongation as a result of dispersion. Additionally there is a significant fall in the amplitude of the received signal in Figure 6c (at 102 kHz), which corresponds to the point where the axial wave's velocity reaches its minimum (refer to Figure 1). This region is also clearly visible on the measured impedance curve of the rod-transducer combination (Figure 6d). Figure 7 contains finite element results at 36 kHz and at 78 kHz, produced using a transient finite element model of the experiment. ABAQUS, a commercial finite element package was used to run the analyses. The graphs have been normalized and the shapes of the graphs can be qualitatively compared to the shapes of the corresponding graphs that appear in Figure 6. The results suggest that FEM can be used to predict the arrival times and relative amplitudes of wave packets in the rod, which is important in characterizing damage in the rod. A comparison of the results obtained from damaged rods will be presented in the following section.

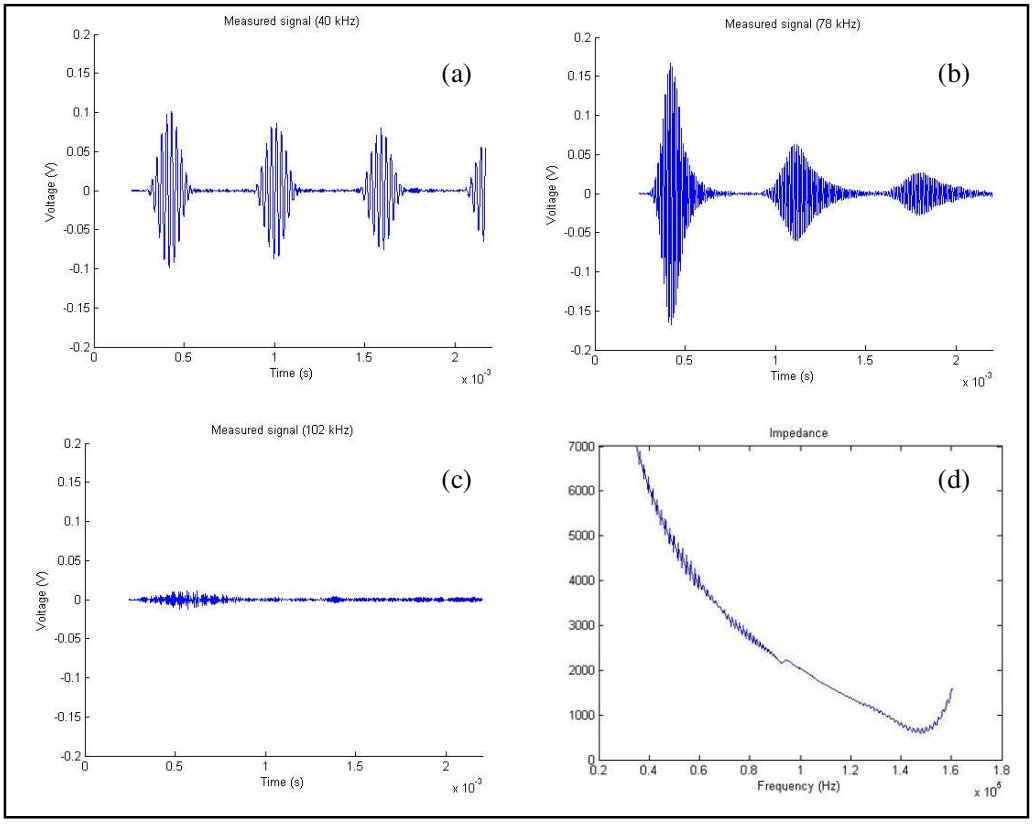


**Figure 6.** Measured responses at different frequencies for windowed excitation signals.

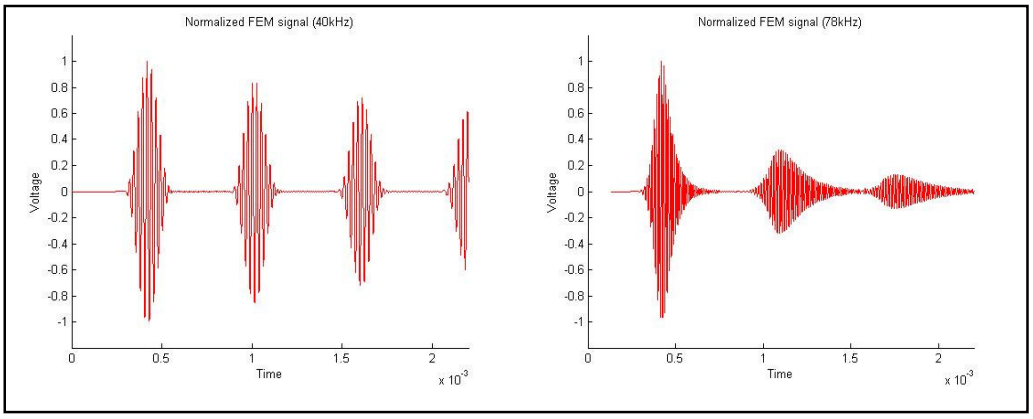


**Figure 7.** Transient finite element simulation of responses.

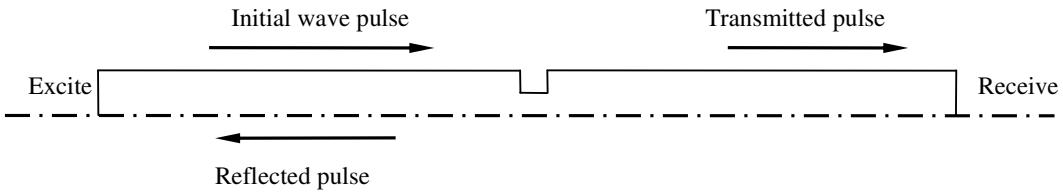


**Figure 8.** Schematic of model used to investigate reflection and transmission coefficients.

## 3. Modelling and measurement of damage in GFRP rods

### 3.1. Estimation of reflection coefficients

Reflections from damage within a waveguide are often quantified by defining reflection and/or transmission coefficients. These coefficients relate the amplitude of the wave reflected from the damage and the wave transmitted past the damage to the amplitude of a datum wave-pulse [5, 12]. In so doing, the severity of the damage can be estimated. Although there are analytical methods for the prediction of such coefficients (see for example [12]) which depend on the mode shape of the wave, these coefficients can practically be quantified by using the time-displacement signals at points along the wave guide, or time-voltage signals at the transducers, provided that a datum signal can be defined and recorded. Figure 8 diagrams the situation. Given that the finite element results qualitatively capture the wave propagation behaviour in the insulator core, the FEM can also be used to provide an indication of the type of signals to be expected when testing rods with various forms of damage. As a prelude to modelling damage, however, the variation in reflection and transmission coefficients with crack size was investigated numerically. An axisymmetric mesh was constructed from which elements were removed to simulate a crack mid-way down the axial length of the model (similar to Figure 8). Piezoelectric actuator discs were also modelled attached to both ends of the rod, and the excitation of a wave packet was simulated by prescribing a varying electrical potential on the excite electrode. Since the model contained no damping, the datum pulse was taken to be the potential signal at the receive electrode in an undamaged model. Five cycles of a 35 kHz signal were used initially, due to the low dispersion at that frequency. The first arrival of a signal at the excite electrode defined the reflected pulse and the first arrival of a signal at the receive electrode defined the transmitted pulse. Windowed Fourier transforms of these signals as well as of the datum signal were taken, and the reflection/transmission coefficients were calculated by dividing the maximum amplitude of the corresponding power spectrum with the maximum value for the datum wave. This was done for various notch sizes. Figure 9a is a plot of the variation in the reflection and transmission coefficients as a function of the notch's axial length at a constant depth. In the graph, the notch's length is expressed as a fraction of the wave length. The upper curve is the reflection coefficient, while the lower denotes the transmission coefficient. The shape of the graph is cyclical because the reflected wave pulse is a superposition of the waves reflected from the front and back surfaces of the crack. As the crack lengthens, the phase between these two waves changes cyclically. For Figure 9a, an effort was made to include the entire wave pulse in the windowed Fourier transform used to calculate the coefficients. The strange unsmooth character of the graph

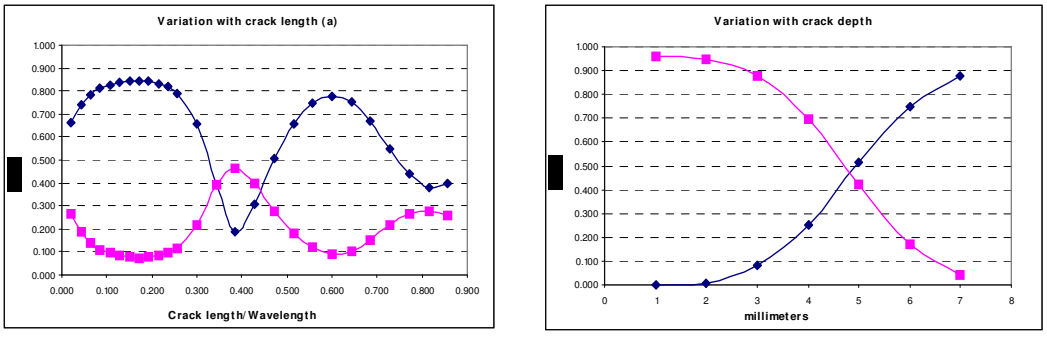


(a) (b)

**Figure 9.** Reflection and transmission coefficients using a wide time window, (a) axial notch of varying length, (b) radial notch of varying depth.

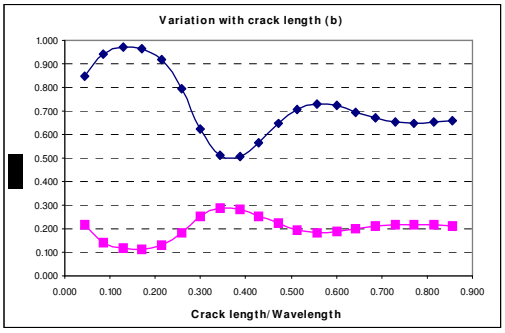


**Figure 10.** Reflection and transmission coefficients of an axial notch using a narrow time window.

comes about because the model was insufficiently long to completely separate all the signals in time. As the crack lengthens, the dispersion characteristics of the rod change and the reflected signal is interfered with by the dispersed reflections off the ends of the rod. Figure 9b shows the variations in the reflection and transmission coefficients as the depth of an infinitely thin radial crack is changed, using the same time window. The concept "infinitely thin" was modelled by disconnecting adjacent elements in the finite element mesh. In the case of an axial notch, when the Fourier window is shortened to include only the first few cycles of the arriving signals, a much smoother curve results (Figure 10). However, the magnitudes of the coefficients change – which serves to illustrate the dependence of the coefficients on the chosen window used to calculate them. Note also that the transmission and reflection coefficients sum to greater than 1 initially. This seems counter to conservation of energy. Bear in mind however that these coefficients are not defined here in terms of energy. That would involve integrating the stress and displacement fields over the area of the rod for the respective pulses as well as taking into account the spread of energy temporally and spatially due to dispersion and defining the appropriate windows. Here we only wish to define coefficients that can be used to quantifiably compare different cracks. Lastly, both graphs exhibit a decaying oscillation. The effect occurs due to the reflection off the two crack surfaces arriving further apart in time at the transducer as the crack lengthens. If a constant temporal window is used, which for the data in Figure 10 is equivalent to the first three cycles of the reflection resulting from the nearest crack surface, progressively less of the energy coming from the farther crack surface is included in the window. Hence the coefficients tend towards those that would occur due to a step down change in geometry. Once again this effect depends intimately on the definition of the window size, but for realistically thin cracks the effect would not be marked.

### 3.2. Rod containing damage

Damage was introduced into the test sample rod in the form of a groove. The groove was machined into the rod at 0.56m down its 1.36m length. It was machined fully circumferentially and its dimensions were 3mm in axial length and 1mm in radial depth. The crack face therefore constitutes 23% of the rod's cross-sectional area. The rod was then tested using the same excitation signals as in the undamaged case. The transducer used in this case consisted of two piezoelectric discs, separated by a short length of GFRP rod. The transducer assembly was bonded to one end of the test sample. One disc in the transducer assembly was used for transmission of the signals, while the other allowed for the simultaneous reception of the excitation and reflection signals. At higher frequencies, the signal was distorted by reflections within the transducer assembly itself, the effect of which can be seen in Figure

11c. Figure 11 shows the measured reflected signal at 40 kHz and 70 kHz and these are compared to the finite element predictions of the received signals. The time signals have been cropped to remove the initial excitation signal. In the FEM models, only a single transducer disc was included. Although the FEM models predict the arrival times of the reflected signals adequately, their magnitudes are somewhat over predicted. For the experiments depicted in Figure 11, the groove was machined into the rod in a position where reflections from the groove would be separated in time from the excitation signal and from the natural reflections of the main wave from the end of the rod. Naturally, reflections resulting from arbitrary damage could just as easily arrive overlapped by signals that do not indicate damage. In order to separate the two, the signals have to be processed in a way that the temporal information in the signal is retained. Wavelet transforms are often used for this purpose, and have been applied to guided wave applications [13]. There remains also a question as to how extensive the damage has to be before it can be detected through "low frequency" ultrasonic means. The answer to this depends not only on the geometry of the crack, but also on the stress distribution within the mode, as the two interact to produce reflections. Figure 12 illustrates the problem. It contains a comparison of the reflected signals received from a damaged and an undamaged rod. Both rods are 240 mm long and are excited using the same transducer at 80 kHz, which excites only the axial mode. The damaged rod contains a thin axial crack purposefully introduced during manufacture. Since the crack runs along the entire length of the rod, any reflected waves would overlap with both the excitation signal and the reflection from the end of the rod. Each plot is averaged from 12 successive measurements. Although small differences are visible between the two curves in Figure 12, nothing as yet can be concluded about the detectability of the crack or the accuracy of the experiment. A suitable signal processing algorithm and more accurate transient modelling are required to advance the

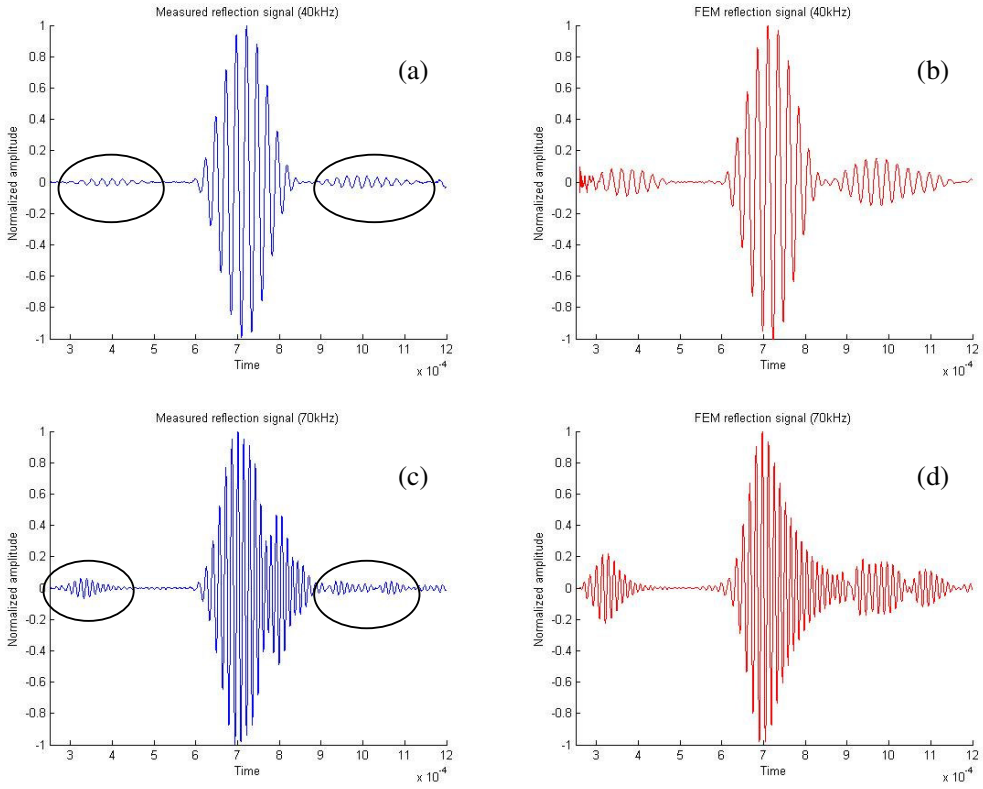


**Figure 11.** Measured and finite element signals for a rod containing damage.

study further.

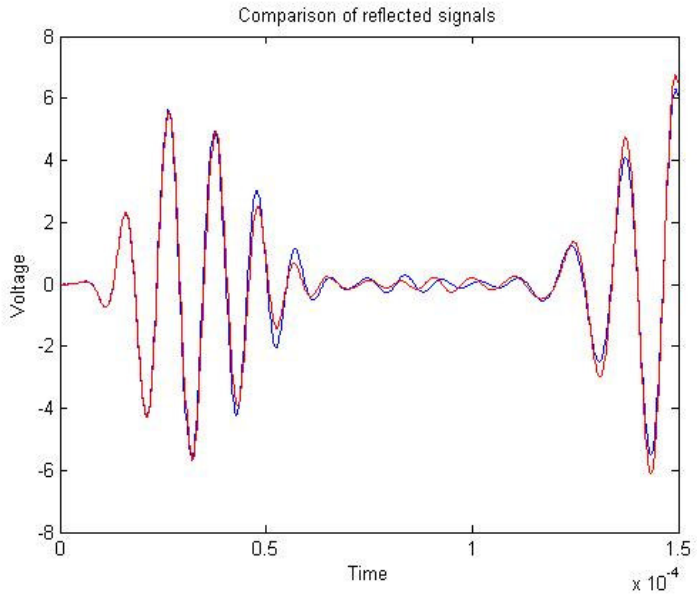


**Figure 12.** Comparison of measured signals from damaged and undamaged short rods.

## 4. Conclusion

Guided wave propagation through transversely isotropic glass fibre reinforced polymer rods has been analysed by the application of the finite element method utilizing waveguide finite elements. This has furnished the frequency dependence of the wave propagation in the rods, which has enabled the selection of an appropriate mode of excitation for practical testing. Additionally, the guided wave analysis allows for a better interpretation of measured signals, since modal velocities and dispersion characteristics are predicted. Numerical and practical experiments have been carried out to verify inspection of a damaged rod. Such experiments show that damage in the rod can be detected from its interaction with guided wave modes. Additionally, said interaction can be modelled qualitatively, even if the material properties of the rod are not initially known, since they can be approximated by iteratively comparing measured wave arrival times and dispersion characteristics with waveguide finite element predictions. However, it is difficult to produce quantitatively correct transient finite element results even with these approximated material parameters, since material damping characteristics and the way in which the transducer is modelled can also introduce errors. The presence of damage results in reflected signals and changes in the transmitted signals, both of which are quantifiable in terms of reflection and transmission coefficients. It has been shown that these coefficients can be defined and recorded in different ways, but they can be used to quantify the extent of damage present in a sample, relative to undamaged samples. The exact values of the coefficients depend on the type of propagating mode, the geometry of the crack and the way in which the signals are processed. Hence, they are relative measures. Practically, sensing damage and estimating its extent would require a signal processing algorithm that preserves time domain information and is able to meaningfully resolve small variations in received signals.

## References


1. Steiner K. V., Eduljee R. F., Huang X. and Gillespie J. W., Ultrasonic NDE techniques for the evaluation of matrix cracking in composite materials. *Composite science and technology*, 53, 193-198, 1995.
2. Prevorovsky Z., Landa M., Blahacek M., Varchon D., Rousseau J., Ferry L. and Perreux D., Ultrasonic scanning and acoustic emission of composite tubes subjected to multiaxial loading. *Ultrasonics*, 36, 531-537, 1998.
3. Rose L. J., Standing on the shoulders of giants: An example of guided wave inspection, *Materials Evaluation (USA)*, 60, 53-59, 2002.
4. Cawley P., Practical long range guided wave inspection – managing complexity. *Review of progress in Quantitative Nondestructive Evaluation*, 657, 22-40, 2003.
5. Cawley P., Lowe M. J. S., Simonetti F., Chevalier C. and Roosenbrand A. G., The variation of the reflection coefficient of extensional guided waves in pipes from defects as a function of defect depth, axial extent, circumferential extent and frequency, *Proceedings of the Institute of Mechanical Engineers Part C: Journal of Mechanical Engineering Science*, 216, 1131-1143, 2002.
6. Alleyne D. N., Pavlakovic B., Lowe M. J. S. and Cawley P., Rapid long range inspection of chemical plant pipework using guided waves. *Insight*, 43, 93-96, 2001.
7. Long R., Lowe M. J. S. and Cawley P., Axisymmetric modes that propagate in buried iron water pipes. *Review of progress in Quantitative Nondestructive Evaluation*, *AIP Conference Proceedings*, 657, 1201-1208, 2003.
8. Loveday P. W., Development of piezoelectric transducers for a railway integrity monitoring system. *Smart Structures and Materials 2000: Smart Systems for Bridges, Structures, and Highways, Proceedings of SPIE*, 3988, 330-338, 2002.
9. Toyama N., Noda J. and Okabe T., Quantitative damage detection in cross-ply laminates using lamb wave method. *Composites and science technology*, 63, 1473-1479, 2003.
10. Gavrić L., Computation of propagative waves in free rail using a finite element technique, *Journal of Sound and Vibration*,185, 531-543, 1995.
11. Hayashi T., Song W. J. and Rose J. L., Guided wave dispersion curves for a bar with an arbitrary cross-section, a rod and rail example. *Ultrasonics*, 41, 175-183, 2003.
12. Lowe M. J. S. and Diligent O., Low-frequency reflection characteristics of the $s_o$ Lamb wave from a rectangular notch in a plate, *Journal of the Acoustical Society of America*, 111, 64-74, 2002.
13. Legendre S., Massicotte D., Goyette J. and Bose T. K., Wavelet-transform-based method of analysis for Lamb-wave ultrasonic NDE signals, *IEEE Transactions on Instrumentation and Measurement*, 49, 524-530, 2000.